Location of objects in multiple-scattering media

P. N. den Outer and Th. M. Nieuwenhuizen

Van der Waals-Zeeman Laboratorium der Universiteit van Amsterdam, Valckenierstraat 65, 1018 XE Amsterdam, The Netherlands

Ad Lagendijk

Van der Waals-Zeeman laboratorium der Universiteit van Amsterdam, Valckenierstraat 65, 1018 XE Amsterdam, The Netherlands, and Fundamenteel Onderzoek der Materie Instituut voor Atoom-en Molecuulfysica, Kruislaan 407, 1098 SJ Amsterdam, The Netherlands

Received March 26, 1992; revised manuscript received October 21, 1992; accepted November 25, 1992

When a small object is placed in a multiple-scattering medium the stationary diffusion equation can be used to derive the disturbance in the transmitted and backscattered light intensity. The diffusion equation will describe the intensity outside and inside the object. The object is characterized by a size, a diffusion constant, and an absorption length. In this way absorbing objects as well as nonabsorbing objects can be treated. The results are derived for two and three dimensions. Experiments are performed on suspended titanium dioxide particles in glycerine, wherein objects could be placed. There is good agreement between theory and experiment. This work shows that with the use of continuous light sources, it may be possible to recover the location of objects accurately inside a diffusive scattering medium.

1. INTRODUCTION

When an object is placed in a highly scattering medium, ballistic light transport from the object to a detector is nearly absent. Direct imaging of the object is impossible, and other methods should be used. Many researchers[1–8] have been attracted by this problem, for which there are important medical applications, such as the location of those tumor cells in human tissue that cannot be seen with conventional techniques (cat scanner, x rays, etc.). As a first step to solving the problem of imaging through scattering media, one could try to reduce the multiple-scattering contribution to the image either by making the media absorb, by filtering out the lowest order of scattering with the help of femtosecond light pulses and ultrafast detection methods,[3,5] or by spatial incoherence techniques.[6] By these methods only the low order of scattered light is detected; therefore high intensities for the incoming light are necessary, and an exponential decay of the signal with increasing distance between the object and boundaries of the scattering medium is to be expected. This puts a severe limit on the probing depth. If one wants to enlarge the probing depth, one should measure the diffuse intensity (i.e., the multiple-scattered light). A good description for light propagation through disordered media can be given by diffusion theory.[9,10] Also, in human tissue light propagates diffusively, and the diffusion approximation can be used to determine, for instance, parameters such as the oxygenation state of tissue.[11–13]

Expressions for the Green's function for the diffusion equation with and without absorption are found,[1,9,14] and in a few simple geometries where absorption is negligible a closed expression can be given (for a spherical geometry see Ref. 15). A closed expression for a two-dimensional slab is derived in this paper.

When the object is small compared with the system size, we show that it is possible to calculate the disturbance on the diffuse intensity. We approach this problem by taking a diffusion constant inside the object that differs from the diffusion constant of the surrounding medium. Also, to characterize the object we introduce a size a and an aborption length l_a or absorption parameter α, describing the situation in which absorption takes place only at the surface of the object. It turns out that one can distinguish between absorbing objects and scattering objects. Scattering objects do not absorb but have a diffusion constant that is different from the surrounding medium.

The important parameter for the visibility of an object is the ratio a/L, a being the size of the object and L the thickness of the system wherein the object has been placed. The local intensity disturbance that is due to the object is diffusively broadened; therefore the visibility is independent of the scattering mean-free path.

To illustrate our approach, we consider a few examples of scattering media confined in a simple geometry. We calculate the transmitted and backscattered intensity for three- and two-dimensional slabs in Subsections 2.A and 2.B, respectively. In Subsection 2.C the disturbance on the diffuse intensity when a point source is used instead of a plane wave is calculated. A spherical geometry is considered in Subsection 2.D. Measurements were carried out for a two-dimensional slab to test the theory. In Section 3 we report our experimental results, which are in good agreement with diffusion theory.

2. CALCULATION OF DIFFUSE INTENSITY

For the transport of light through a scattering medium and through an object we use the diffusion approximation, and we take smooth boundaries for medium and object. We consider a spherical object with a radius a that is small compared with the system size L. Our goal is to solve the

0740-3232/93/061209-10$06.00

stationary diffusion equation with boundary conditions given by the geometry of the scattering medium and extra boundary conditions from the embedded object. We consider a slab geometry and a spherically shaped geometry. The slab is situated between $x = L$ and $x = 0$ and is infinitely extended in the yz plane. A source $S(y, z)$, plane wave or pointlike, is placed at $x = L$. The sphere that confines the scattering medium is centered at the origin. The stationary diffusion equation reads as

$$\Delta I(\mathbf{r}) = 0. \tag{1}$$

The boundary conditions at the outer surfaces of the medium are for a slab

$$I(L, y, z) = S(y, z), \qquad I(0, y, z) = 0 \tag{2}$$

and for a sphere

$$I(R, \theta, \phi) = S(\theta, \phi), \tag{3}$$

where $I(\mathbf{r})$ is the diffuse intensity, L is the thickness of the slab, and R is the radius of the sphere.

One can distinguish at least two means of absorption by the object: uniform absorption in its volume or absorption only at its surface. Absorption at the surface could be used, for instance, as a model for dyed polystyrene spheres. For uniform absorption an absorption length $l_a \equiv 1/\kappa$ can be introduced, and for the intensity inside the object the diffusion equation

$$\Delta I(\mathbf{r}) = \kappa^2 I(\mathbf{r}) \tag{4}$$

should be considered. In this case the problem is to solve Eqs. (1) and (4), together with the boundary condition given by Eq. (2) or (3) and with extra boundary conditions on the surface of the object that are given by

$$I_{\text{out}}(a^+) = I_{\text{in}}(a^-), \tag{5}$$

$$D_1 \frac{\partial I_{\text{out}}}{\partial n}\bigg|_{a^+} = D_2 \frac{\partial I_{\text{in}}}{\partial n}\bigg|_{a^-}. \tag{6}$$

The diffusion constants D_1 and D_2 are for the medium and for inside the object, respectively. The normal derivative $\partial/\partial n$ is taken on the surface of the object. Equation (5) provides continuity of intensity, and Eq. (6) conserves the flux through the boundary of the object. These boundary conditions follow from the underlying transport theory, which yields both the diffusion equation and its boundary conditions.

To account for absorption only at the boundary of the object, one modifies Eq. (6) such that the flux is not conserved. In this way absorption takes place at the boundary of the object, and we can use Eq. (1) for the intensity inside the object. The modified boundary conditions are

$$I_{\text{out}}(a^+) = I_{\text{in}}(a^-), \tag{7}$$

$$D_1 \frac{\partial I_{\text{out}}}{\partial n}\bigg|_{a^+} = D_2 \frac{\partial I_{\text{in}}}{\partial n}\bigg|_{a^-} + \alpha I_{\text{in}}(a). \tag{8}$$

The absorption parameter α has the dimension of speed

We can distinguish a number of relevant cases. For instance,

$\alpha = \kappa = 0,\ D_2 \neq D_1$:	pure scatterer, no absorption,
$\alpha = \kappa = 0,\ D_2 = \infty$:	glass object or air bubble,
$\alpha \neq 0$, or $\kappa \neq 0$:	absorber, absorbing behavior dominates scattering.

Since Eq. (1) is a Laplace equation, we can use the formalism of electrostatics and introduce the analog of charges, dipoles, and their mirror images. Positive charges describe light sources and negative sources describe absorption of light. Dipoles describe scattering objects.

A. Three-Dimensional Slab

We consider a plane wave $S(L, y, z) = I_0$ incident upon a slab. A schematic view is given in Fig. 1. A spherical object with radius a is located at $\mathbf{r}_0 = (x_0, 0, 0)$. We must write the potential for a point charge and apply the boundary condition given by Eq. (2), with $S(y, z) = 0$. This results in a summation over mirror images, the outcome being the diffusion propagator for a slab. The potential for a dipole can easily be obtained from this result if one takes the derivative with respect to the position of the charge. The intensity in the slab can be expressed as

$$\begin{aligned} I(\mathbf{r}) = I_0 \frac{x}{L} &+ q \sum_{n=-\infty}^{\infty} \frac{1}{|\mathbf{r} - r_0 + 2Ln\hat{x}|} - \frac{1}{|\mathbf{r} + r_0 + 2Ln\hat{x}|} \\ &+ p \sum_{n=-\infty}^{\infty} \frac{x - x_0 + 2nL}{[(x - x_0 + 2nL)^2 + \rho^2]^{3/2}} \\ &+ \frac{x + x_0 + 2nL}{[(x + x_0 + 2nL)^2 + \rho^2]^{3/2}}, \end{aligned} \tag{9}$$

with $\hat{x}$ being a unit vector along the x axis and $\rho^2 = y^2 + z^2$.

The first term in Eq. (9) describes the undisturbed intensity, the second term represents the effect of absorption analogous to a charge in electrodynamics, and the

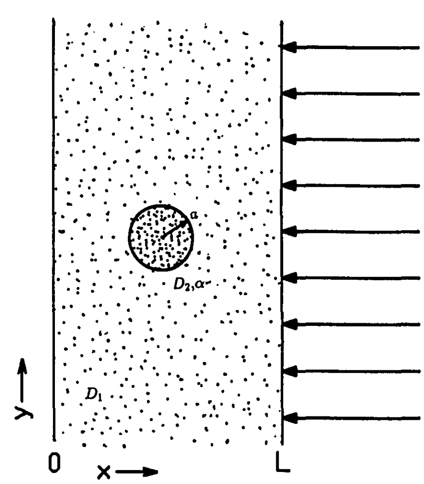

Fig. 1. Schematic view of a multiple-scattering system with an embedded spherical object. The scattering system is characterized by a diffusion constant D_1 and the object by radius a, diffusion constant D_2, and absorbing parameter α. A plane wave is incident at $x = L$. The intensity is derived at $x = 0$ and $x = $ L.

third is the dipole term from scattering. Further details of the object will be found in higher multipoles for the intensity outside the object, but their contribution to the disturbance far from the object will be small. When $a \ll L$, it is sufficient to retain only the first two multipoles.

The ansatz for the intensity inside the object depends on whether we take uniform absorption or absorption only at the boundary of the object. When we introduce an absorbing length l_a, the ansatz for the intensity inside the object is given by the first two spherical Bessel functions with imaginary arguments

$$I_{\text{in}}(\mathbf{r}) = A\frac{\sinh \kappa r}{\kappa r} - \frac{3B}{\kappa}\left(\frac{\sinh \kappa r}{\kappa^2 r^2} - \frac{\cosh \kappa r}{\kappa r}\right)Y_{10}(\theta, \phi), \tag{10}$$

where $Y_{10}(\theta, \phi) = \cos\theta$ is the spherical harmonic with $l = 1, m = 0$.

If the object absorbs only at its boundary, we can take for the intensity inside the object in leading order a linear solution of the diffusion equation

$$I_{\text{in}}(\mathbf{r}) = A + B(x - x_0). \tag{11}$$

For small κ Eq. (10) shows similar behavior,

$$\lim_{\kappa \to 0} I_{\text{in}}(\mathbf{r}) = A + \left(\frac{-3B}{\kappa}\right)\left(\frac{-\kappa r}{3}\right)\left(\frac{x - x_0}{r}\right). \tag{12}$$

Note that we have chosen θ to be the angle between $\mathbf{r}$ and the x axis.

Most general is to allow both for uniform absorption and for absorption at the surface, so that ansatz is given by Eq. (10) and the boundary conditions by Eqs. (7) and (8).

When Eq. (9) is approximated for $\mathbf{r}$ close to r_0, the equation reduces to

$$I(\mathbf{r}) \approx I_0\frac{x}{L} + q\left[\frac{1}{|\mathbf{r} - \mathbf{r}_0|} + O\left(\frac{a}{L}\right)\right] + p\left[\frac{x - x_0}{|\mathbf{r} - \mathbf{r}_0|^3} + O\left(\frac{a}{L}\right)\right]. \tag{13}$$

A straightforward calculation gives for the coefficients

$$q = -I_0\frac{a x_0}{L}\frac{D_2(\cosh \kappa a - \operatorname{sinhc} \kappa a)/\operatorname{sinhc} \kappa a + \alpha a}{D_1 + D_2(\cosh \kappa a - \operatorname{sinhc} \kappa a)/\operatorname{sinhc} \kappa a + \alpha a},$$

$$p = I_0\frac{a^3}{L}\frac{D_1 - D_2(2\cosh \kappa a - 2\operatorname{sinhc} \kappa a - \kappa a \sinh \kappa a)/(\operatorname{sinhc} \kappa a - \cosh \kappa a) - \alpha a}{2D_1 + D_2(2\cosh \kappa a - 2\operatorname{sinhc} \kappa a - \kappa a \sinh \kappa a)/(\operatorname{sinhc} \kappa a - \cosh \kappa a) + \alpha a},$$

$$A = \frac{D_1 q}{\alpha a^2 \operatorname{sinhc} \kappa a + A d_2(\cosh \kappa a - \operatorname{sinhc} \kappa a)},$$

$$B = \frac{1}{3}\frac{\kappa^2 a^2}{\operatorname{sinhc} \kappa a - \cosh \kappa a}\left(\frac{I_0}{L} + \frac{p}{a^3}\right), \tag{14}$$

where $\operatorname{sinhc} x \equiv \sinh(x)/x$. When κ becomes small, these expressions reduce to

$$q = -I_0\frac{x_0 a}{L}\frac{\alpha a}{D_1 + \alpha a},$$

$$p = I_0\frac{a^3}{L}\frac{D_1 - D_2 - \alpha a}{2D_1 + D_2 + \alpha a},$$

$$A = \frac{D_1 q}{\alpha a^2},$$

$$B = \frac{I_0}{L} + p\frac{1}{a^3}. \tag{15}$$

Within the diffusion approach the transmitted and backscattered light is defined by the intensity at $x = l$ and $x = L - l$, with l being the transport mean-free path.[16] So the transmitted intensity is given by

$$\begin{aligned} T(\rho) &\equiv \frac{l}{I_0}\frac{\partial I}{\partial x}\bigg|_{x=0} \\ &= \frac{l}{L} + 2ql\sum_{n=-\infty}^{\infty}\frac{x_0 + 2nL}{[(x_0 + 2nL)^2 + \rho^2]^{3/2}} \\ &\quad + 2pl\sum_{n=-\infty}^{\infty}\frac{\rho^2 - 2(x_0 + 2nL)^2}{[(x_0 + 2nL)^2 + \rho^2]^{5/2}} \end{aligned} \tag{16}$$

and the backscattered intensity by

$$\begin{aligned} B(\rho) &\equiv 1 - \frac{l}{I_0}\frac{\partial I}{\partial x}\bigg|_{x=L} \\ &= 1 - \left(\frac{l}{L} + 2ql\sum_{n=-\infty}^{\infty}\frac{x_0 + L(2n+1)}{\{[x_0 + L(2n+1)]^2 + \rho^2\}^{3/2}}\right. \\ &\quad \left. + 2pl\sum_{n=-\infty}^{\infty}\frac{\rho^2 - 2[x_0 + (2n+1)L]^2}{\{[x_0 + (2n+1)L]^2 + \rho^2\}^{5/2}}\right). \end{aligned} \tag{17}$$

When the object does not absorb ($\alpha = 0$ and $\kappa = 0$), only the dipole term in Eqs. (16) and (17) is present. The strength of the dipole term, the peak height relative to background, is of order a^3/L^3. When absorption is present, we usually have $\alpha a \gg D_1 a^2/L^2$ ($a \ll L$), in which case the charge term dominates with strength a/L. From Eqs. (16) and (17) we see further that the absolute strength of the disturbance on the backscattered and transmitted intensity is equal, but in transmission the strength is more pronounced, since it is superimposed upon a much lower background.

At this point we can compare our results with a prediction of Berkovits and Feng.[7] These authors base a model on one nonabsorbing static particle embedded in a sea of moving particles. We can mimic this situation by setting a small and $\alpha = \kappa = 0$ in Eq. (16), which gives a small dipole disturbance in the intensity. In Ref. 7 it is claimed that the static particle will act as a light source with unit strength and independent of the particle size. This contradicts our result. We do not see how the effect of a light source can be explained from a physical mechanism.

Moreover, a careful reinvestigation of the diagrammatic analysis employed in Ref. 7 reveals that the result indeed has the behavior of a dipole rather than of a charge.

B. Two-Dimensional Slab

The disturbance on the intensity for a two-dimensional slab is derived completely analogously to the previous approach. To obtain the intensity distribution from a point source in a two-dimensional system, one has to write down the potential for a line charge and apply the first boundary condition of Eqs. (2) with $S(L, y, z) = 0$. Experimentally a two-dimensional system can be realized if one makes the system translationally invariant along one coordinate; i.e., if one uses rods and glass fibers as objects. The application of the boundary condition of Eqs. (2) on the potential for a line charge results in a summation over mirror images, which can be performed exactly. Here it is convenient to introduce the complex variable $\zeta \equiv x + iy$. The potential for a line dipole can again be found if one takes the derivative of this result with respect to the position. The ansatz for the solution of the diffusion equation [Eq. (1)] with a line charge and a line dipole outside the object reads as

$$I_{\text{out}}(\zeta) = I_0 \frac{x}{L} + q\,\text{Re}\left\{\ln \frac{\sin[(\pi/2L)(\zeta - x_0)]}{\sin[(\pi/2L)(\zeta + x_0)]}\right\} + p\,\text{Re}\left\{\cot\left[\frac{\pi}{2L}(\zeta - x_0)\right] + \cot\left[\frac{\pi}{2L}(\zeta + x_0)\right]\right\}, \tag{18}$$

where x_0 is the position of the scatterer ($y_0 = 0$). For absorption only at the boundary the ansatz is

$$I_{\text{in}}(\zeta) = A + B(x - x_0). \tag{19}$$

For uniform absorption the ansatz for the intensity inside the object is

$$I_{\text{in}}(\zeta) = AI_0(\kappa\rho) + \frac{2B}{\kappa} I_1(\kappa\rho)\cos\phi. \tag{20}$$

Here $I_0(r)$ and $I_1(r)$ are the modified Bessel functions of order 0 and 1, $\rho = |\boldsymbol{\rho}| = (x^2 + y^2)^{1/2}$, and ϕ is the angle between $\boldsymbol{\rho}$ and the x axis.

To obtain the constants q, p, A, and B we approximate Eq. (18) for ζ close to x_0 and for a/L small:

$$I_{\text{out}}(\zeta) = I_0 \frac{x_0 + (x - x_0)}{L} + q\left\{\ln \frac{\pi}{2L} \frac{[(x - x_0)^2 + y^2]^{1/2}}{\sin(\pi/L)x_0} + O\left(\frac{a^2}{L^2}\right)\right\} + p\left\{\frac{2L(x - x_0)}{\pi[(x - x_0)^2 + y^2]^{1/2}} + \cot\frac{\pi}{L}x_0 + O\left(\frac{a}{L}\right)\right\}. \tag{21}$$

We insert Eqs. (19) and (21) into Eqs. (7) and (8), which accounts for uniform absorption and absorption on the surface of the object, to obtain

$$\begin{aligned} q &= I_0\left[\frac{x_0}{L} + p\cot(\pi x_0/L)\right] \times \frac{\alpha a + D_2\kappa a I_1(\kappa a)/I_0(\kappa a)}{D_1 + [\alpha a + D_2\kappa a I_1(\kappa a)/I_0(\kappa a)]\ln(L/a^*)}, \\ p &= I_0 \frac{\pi a^2}{2L^2} \frac{D_1 - D_2[\kappa a I_0(\kappa a) - I_1(\kappa a)]/I_1(\kappa a) - \alpha a}{D_1 + D_2[\kappa a I_0(\kappa a) - I_1(\kappa a)]/I_1(\kappa a) + \alpha a}, \\ A &= \frac{I_0(\kappa a)}{\kappa a I_1(\kappa a) D_2 + I_0(\kappa a)\alpha a} D_1 q, \\ B &= \frac{\kappa a}{2I_1(\kappa a)}\left(I_0\frac{1}{L} + p\frac{2L}{\pi a^2}\right), \end{aligned} \tag{22}$$

with the rescaled radius

$$a^* = \frac{\pi a}{2\sin(\pi x_0/L)}. \tag{23}$$

Although the dipole term depends on α and κ separately, we take $\kappa = 0$ from now on. This simplification is justified because the dipole contribution to the intensity disturbance can be neglected whenever absorption is present. One may conclude that the intensity disturbance far outside the object does not depend dramatically on specific mechanism of absorption. For $\kappa = 0$, the coefficients reduce to

$$\begin{aligned} q &= I_0\left[\frac{x_0}{L} + \cot(\pi x_0/L)\frac{D_1 - D_2 - \alpha a}{D_1 + D_2 + \alpha a}\frac{\pi a^2}{2L^2}\right] \times \frac{\alpha a}{D_1 + \alpha a \ln(L/a^*)}, \\ p &= I_0 \frac{D_1 - D_2 - \alpha a}{D_1 + D_2 + \alpha a}\frac{\pi a^2}{2L^2}, \\ A &= \frac{D_1 q}{\alpha a}, \\ B &= I_0\frac{1}{L} + p\frac{2L}{\pi a^2}. \end{aligned} \tag{24}$$

When $\alpha a > D_1 a^2/L^2$, the charge term dominates and has strength $[\ln(L/a^*) + D_1/\alpha a]^{-1}$. We obtain for the transmitted light

$$\begin{aligned} T(y) &\equiv \frac{l}{I_0}\frac{\partial I(\mathbf{r})}{\partial x}\bigg|_{x=0}, \\ &= \frac{l}{L}\left[1 - q\frac{\pi\sin(\pi x_0/L)}{\cosh(\pi y/L) - \cos(\pi x_0/L)}\right. \\ &\equiv \left. - 2\pi p\frac{1 - \cosh(\pi y/L)\cos(\pi x_0/L)}{[\cosh(\pi y/L) - \cos(\pi x_0/L)]^2}\right] \end{aligned} \tag{25}$$

and for the backscattered light

$$\begin{aligned} B(y) &\equiv 1 - \frac{l}{I_0}\frac{\partial I(\mathbf{r})}{\partial x}\bigg|_{x=L}, \\ &= 1 - \frac{l}{L}\left[1 + q\frac{\pi\sin(\pi x_0/L)}{\cosh(\pi y/L) + \cos(\pi x_0/L)}\right. \\ &\quad \left. - 2\pi p\frac{1 + \cosh(\pi y/L)\cos(\pi x_0/L)}{[\cosh(\pi y/L) + \cos(\pi x_0/L)]^2}\right]. \end{aligned} \tag{26}$$

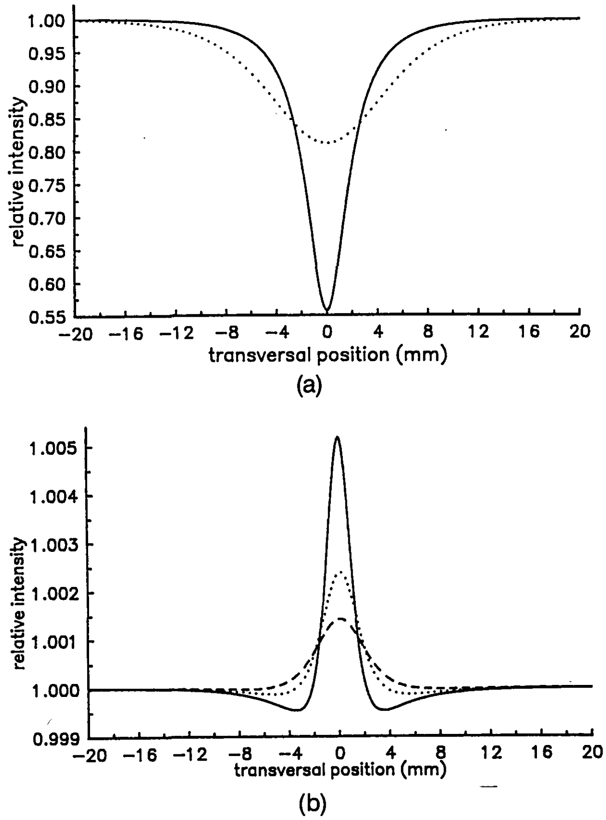

Fig. 2. Calculated diffuse intensities are shown for an object embedded in a two-dimensional multiple scattering system, as a function of the transversal distance to the object. The intensity is plotted relative to the undisturbed intensity (no object present), according to Eq. (26). (a) Transmission for absorbing rod, $a = l, \alpha = \infty, \kappa = 0$. Solid curve, $x_0 = 20\ l$; dotted curve, $x_0 = 80\ l$. (b) Transmission for scattering rod, $a = l, \alpha = \kappa = 0$, $D_2 = \infty$. Solid curve, $x_0 = 20\ l$; dotted curve, $x_0 = 30\ l$; dashed curve, $x_0 = 40\ l$. In all cases $L = 100\ l$. L is the thickness of the slab, and l is the mean free path.

A few examples are plotted in Fig. 2 for different positions and absorption coefficients.

C. Point Source

It is often more convenient to use a point source instead of a plane wave, and also the quality of the image can be improved when the response of the system on a point source is known.[17] To calculate this response, first one should know the intensity distribution in the slab that is due to the point-source incidence in the absence of an object. According to Akkermans *et al.*,[16] one can make the assumption that all the incoming light starts to propagate diffusely at one transport mean free path inside the slab. Without an object, the intensity distribution inside the slab is given by

$$G(l,\zeta) = \mathrm{Re}\left\{\ln \frac{\sin[(\pi/2L)(\zeta - l)]}{\sin[(\pi/2L)(\zeta + l)]}\right\} \tag{27}$$

for a two-dimensional system and by

$$G(l,\mathbf{r}) = \sum_{n=-\infty}^{\infty} \frac{1}{[(l - x + 2Ln)^2 + y^2 + z^2]^{1/2}} - \frac{1}{[(l + x + 2Ln)^2 + y^2 + z^2]^{1/2}} \tag{28}$$

for a three-dimensional system. Since a point source is used, the ansatz for the solution of the total problem, medium plus object, will change. One should realize that the direction of the dipole depends on the local light flux. The direction of the flux at a particular point is now a function of position. The new ansatz in two dimensions reads as

$$\begin{aligned} I_{\mathrm{out}}(\zeta) = I_0 G(l,\zeta) &+ q\,\mathrm{Re}\left\{\ln \frac{\sin[(\pi/2L)(\zeta - x_0 - iy_0)]}{\sin[(\pi/2L)(\zeta + x_0 + iy_0)]}\right\} \\ &+ \mathrm{Re}\left\{p \cot\left[\frac{\pi}{2L}(\zeta - x_0 + iy_0)\right]\right. \\ &\left. + p^* \cot\left[\frac{\pi}{2L}(\zeta + x_0 - iy_0)\right]\right\}, \end{aligned} \tag{29}$$

with

$$p \equiv \hat{p}s_1(x_0, y_0) + i\hat{p}s_2(x_0, y_0). \tag{30}$$

The coefficients $s_1(x_0, y_0)$ and $s_2(x_0, y_0)$ follow from a first-order Taylor expansion,

$$\begin{aligned} s_1 &= \frac{\sin[(\pi/L)(x_0 - l)]}{\cosh[(\pi/L)y_0] - \cos[(\pi/L)(x_0 - l)]} - \frac{\sin[(\pi/L)(x_0 + l)]}{\cosh[(\pi/L)y_0] - \cos[(\pi/L)(x_0 + l)]}, \\ s_2 &= \frac{\sinh[(\pi/L)y_0]}{\cosh[(\pi/L)y_0] - \cos[(\pi/L)(x_0 - l)]} - \frac{\sinh[(\pi/L)x_0]}{\cosh[(\pi/L)y_0] - \cos[(\pi/L)(x_0 - l)]}. \end{aligned} \tag{31}$$

Also, the intensity inside the object should be adjusted to the local flux direction:

$$I_{\mathrm{in}} = A + B[s_1(x_0, y_0)(x - x_0) + s_2(x_0, y_0)(y - y_0)]. \tag{32}$$

Now one can perform a straightforward calculation to obtain the coefficients $q, \hat{p}, A$, and B. They are

$$\begin{aligned} q &= [I_0 G(l,\zeta_0) + \hat{p}s_1(x_0, y_0)\cot(\pi x_0/L)]\frac{\alpha a}{D_1 + \alpha a \ln(L/a^*)}, \\ \hat{p} &= I_0\left(\frac{\pi a}{2L}\right)^2 \frac{D_1 - D_2 - \alpha a}{D_1 + D_2 + \alpha a}, \\ A &= D_1 q/\alpha a, \\ B &= I_0 \frac{\pi}{2L}\frac{2D_1}{D_1 + D_2 + \alpha a}. \end{aligned} \tag{33}$$

In three dimensions the new ansatz reads as

$$I_{\mathrm{out}}(\mathbf{r}) = I_0 G(l,\mathbf{r}) + qI_q(\mathbf{r}) + p\frac{\partial}{\partial \mathbf{r}}\bigg|_{\mathbf{r}_0} G(l,\mathbf{r}) \cdot \frac{\partial}{\partial \mathbf{r}_0} I_q(\mathbf{r}), \tag{34}$$

$$I_{\mathrm{in}}(\mathbf{r}) = A + B(\mathbf{r} - \mathbf{r}_0) \cdot \frac{\partial}{\partial \mathbf{r}}\bigg|_{\mathbf{r}_0} G(l,\mathbf{r}), \tag{35}$$

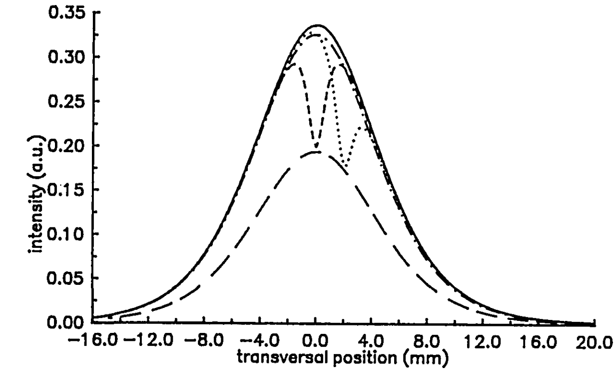

Fig. 3. Calculated transmitted diffuse intensities as a function of the transversal distance y for a slab containing an absorbing spherical object at various positions, following Eq. (16). The light source is pointlike and placed at $\mathbf{r} = (l, 0, 0)$. Slab thickness $L = 50\ l$, absorbing object radius $a = l, \alpha = \infty$, scattering term neglected. Solid curve, no object; long-dashed curve, $x_0 = 45\ l, y_0 = 0$; dashed-dotted curve, $x_0 = 45\ l, y_0 = 10\ l$; short-dashed curve, $x_0 = 5\ l, y_0 = 0$; dotted curve $x_0 = 5\ l, y_0 = 10\ l$.

where

$$I_q(\mathbf{r}) \equiv \sum_{n=-\infty}^{\infty} \frac{1}{[(x - x_0 + 2Ln)^2 + (y - y_0)^2 + (z - z_0)^2]^{1/2}} - \frac{1}{[(x + x_0 + 2Ln)^2 + (y - y_0)^2 + (z - z_0)^2]^{1/2}}. \tag{36}$$

The coefficients q, p, A, and B follow again from boundary conditions (7) and (8). This results in

$$\begin{aligned} q &= -aI_0G(l, \mathbf{r}_0)\frac{\alpha a}{D_1 + \alpha a}, \\ p &= a^3I_0\frac{D_1 - D_2 - \alpha a}{2D_1 + D_2 + \alpha a}, \\ A &= \frac{D_1 q}{\alpha a^2}, \\ B &= I_0\frac{3D_1}{2D_1 + D_2 + \alpha a}. \end{aligned} \tag{37}$$

$$q = -a\left[I_0G_R(\mathbf{r}_s, \mathbf{r}_0) - \mathbf{p}\cdot\mathbf{r}_0\frac{R}{(r_0^2 - R^2)^2}\right]\frac{\alpha a}{D_1 + \alpha a[1 - aR/(r_b^2 - R^2)]}, \tag{42}$$

$$\begin{aligned} \mathbf{p} = {} & a^3I_0\frac{\partial}{\partial\mathbf{r}}\bigg|_{\mathbf{r}_0} G_R(\mathbf{r}, \mathbf{r}_s)\frac{D_1 - D_2 - \alpha a}{2D_1[1 - ½a^3R^3/(r_0^2 - R^2)^3] + (D_2 + \alpha a)[1 + a^3R^3/(r_0^2 - R^2)^3]} \\ & + q\mathbf{r}_0\frac{R}{r_0^2 - R^2}\frac{D_1 + D_2 + \alpha a}{2D_1[1 - ½a^3R^3/(r_0^2 - R^2)^3] + (D_2 + \alpha a)[1 + a^3R^3/(r_0^2 - R^2)^3]}, \end{aligned} \tag{43}$$

$$A = -\frac{D_1 q}{\alpha a^2}, \tag{44}$$

$$\mathbf{B} = I_0\frac{\partial}{\partial\mathbf{r}}\bigg|_{\mathbf{r}_0} G_R(\mathbf{r}, \mathbf{r}_s)q\mathbf{r}_0\frac{R}{(r_0^2 - R^2)^2} + \mathbf{p}\left[\frac{1}{a^3} + \frac{R^3}{(r_0^2 - R^2)^3}\right]. \tag{45}$$

The disturbance on the intensity depends strongly on the position of the light source. The disturbance can be more pronounced than for plane-wave incidence, depending on the relative distance between the object and the light source. This is a more convenient situation because now a displacement of the source can give either a background measurement (without an object) or a measurement with an object. A few examples are plotted in Fig. 3. The transmitted intensity is plotted for various positions of the object with respect to the point source and the boundaries of the slab. The strong dependence of the transmitted intensity on the position of the object is readily seen from the figure.

D. Spherical Geometry

An expression for the light intensity is derived for a spherical medium in which an object has been placed. First we must know the diffusion propagator, or the Green's function, for a sphere. When absorption is absent or negligible, a closed expression can easily be obtained with the help of only one mirror image.[15] We will use this Green's function to calculate the disturbance. A point source is used and placed at the positive z axis at one transport mean-free path underneath the surface of the sphere[16]: $\mathbf{r}_s = (0, 0, R - l)$. So the intensity inside the sphere of radius R, in the absence of an object, is given by

$$I(\mathbf{r}) = I_0G_R(\mathbf{r}, \mathbf{r}_s). \tag{38}$$

The Green's function for a sphere is given by

$$G_R(\mathbf{r}_1, \mathbf{r}_2) = \left[\frac{1}{|\mathbf{r}_1 - \mathbf{r}_2|} - \frac{R}{r_2}\frac{1}{\left|\mathbf{r}_1 - \frac{R^2}{r_2^2}\mathbf{r}_2\right|}\right]. \tag{39}$$

When an object is placed at $\mathbf{r}_0$ inside the sphere, we can express the intensity as

$$I_{\text{out}}(\mathbf{r}) = I(\mathbf{r}) + qG_R(\mathbf{r}, \mathbf{r}_0) - \mathbf{p}\cdot\frac{\partial}{\partial\mathbf{r}_0}G_R(\mathbf{r}, \mathbf{r}_0). \tag{40}$$

Inside the sphere we use the ansatz

$$I_{\text{in}} = A + I_0\mathbf{B}\cdot(\mathbf{r} - \mathbf{r}_0). \tag{41}$$

We use boundary conditions (7) and (8) to derive the coefficients

The coefficients q and $\mathbf{p}$ are still to be obtained from Eqs. (42) and (43). But the above form permits an easy comparison with the former obtained coefficients. The transmission through the surface of the sphere can be found if one takes the normal derivative.

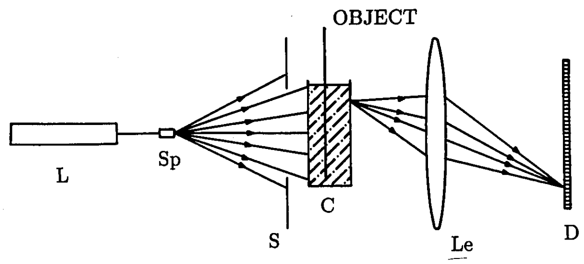

Fig. 4. Experimental setup: L, laser, Sp, spatial filter; S, screen; C, cell with the scattering medium and the object; Le, lens for imaging the diffuse intensity on D, the one-dimensional diode array.

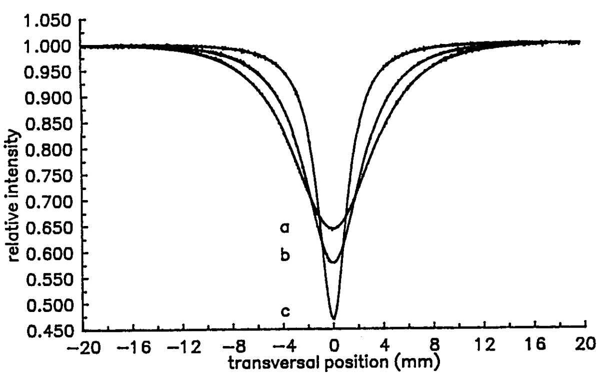

Fig. 5. Transmitted intensity profiles from a cell containing a diffusive scattering suspension, for various positions of the embedded absorbing wire $\phi = 350$ μm: a, $x_0 = 1.00$ mm; b, $x_0 = 2.60$ mm, and c, $x_0 = 4.10$ mm. The experimental data are shown together with the best numerical fits for Eq. (25): a, $x_0 = 1.41 \pm 0.05$ mm, $D_1/\alpha a = 0.95 \pm 0.03$; b, $x_0 = 2.86 \pm 0.05$ mm, $D_1/\alpha a = 1.04 \pm 0.03$; c, $x_0 = 4.33 \pm 0.05$ mm, $D_1/\alpha a = 1.11 \pm 0.03$. In all cases $a = 0.175$, $p = 0$, $l = 20 \pm 3$ μm, and cell thickness $L = 10.0$ mm.

3. MEASUREMENTS

The experimental setup for a plane-wave transmission measurement is shown in Fig. 4. A 7-mW continuous-wave He–Ne laser beam ($\lambda = 633$ nm) is spatially filtered and expanded to a radius of approximately 20 cm to produce a flat beam profile. Part of this beam impinges upon the cell with the object in the highly scattering medium. The transmitted light, imaged on a one-dimensional diode array, is read out by a computer. The spatial resolution is approximately 60 μm. When backscattering experiments are done, the illuminated side of the cell is imaged on the diode array. Care should be taken for the window reflection of the cell. We have used two different cells. The first has a thickness of 4 mm and 4 mm × 40 mm × 40 mm sized windows, the second has a variable thickness of 5 or 10 mm and windows with size 20 mm × 60 mm × 60 mm. Complications are introduced by the glass windows, since light is totally reflected by the window–air interface when the angle between the surface normal and the light ray is beyond the critical angle. This reflected light either enters the sample again or is reflected by it. As a consequence, every point source at the boundary of the scattering medium is spread out in a triangular intensity profile, and a nonnegligible deformation of the intensity occurs. Transmission experiments on absorbing objects suffer most from this effect, because the intensity profile relative to the background is the largest.

This deformation can be reproduced if one convolutes the calculated profiles with the triangular intensity profile. The latter should be calculated on the basis of multiple reflections inside the window. However, this will extend the fitting procedure by the introduction of more fit parameters, and therefore the procedure is not favorable.

We have chosen to reduce the effect of these reflections on the intensity profile by using a cell with thick windows. The total internal reflected light is well separated from its source, and in most cases the light is reflected beside the sample. (An antireflection coating on the windows would not have solved this problem because the coating cannot reduce total internal reflections.)

For plane-wave incident experiments we perform ratio measurements to correct for the sensitivity of the individual diodes and to correct for the remaining beam profile. Depending on the strength of the signal, integration times vary from 10 s to 3 min. The scattering medium consists of suspended TiO_2 rutile particles, having an average size of 220 nm, in glycerine. We calculate the transport mean-free path from the measured scattering mean-free path by means of Mie theory.[10]

In Fig. 5 we present transmission measurements for absorbing rods. We use a 0.35-mm pencil embedded in a scattering medium with a transport mean-free path of 20 μm. The thickness of the cell is 10.0 mm. The solid curves are the best numerical fits of Eq. (25) to the measured profiles. Here the position and the absorbing

Table 1. Fits of the Calculated Line Shape to Experimental Data Obtained from a Transmission Experiment with an Absorbing Rod[a]

Experimental Normal Position (mm)	Fitted Normal Position (mm)	Absorption Strength $D_1/\alpha a$	Experimental Position Relative to First Position (mm)	Fitted Position Relative to First Position (mm)
0.75 ± 0.05	1.23 ± 0.02	0.95 ± 0.03	0	0
1.40 ± 0.05	1.91 ± 0.02	0.99 ± 0.03	0.65 ± 0.07	0.68 ± 0.03
2.30 ± 0.05	2.78 ± 0.02	1.04 ± 0.03	1.55 ± 0.07	1.55 ± 0.03
3.50 ± 0.05	3.91 ± 0.02	1.10 ± 0.03	2.75 ± 0.07	2.68 ± 0.03
4.95 ± 0.05	5.28 ± 0.02	1.11 ± 0.03	4.20 ± 0.07	4.05 ± 0.03
6.30 ± 0.05	6.67 ± 0.02	0.96 ± 0.03	5.55 ± 0.07	5.44 ± 0.03
7.80 ± 0.05	8.2 ± 0.1	0.8 ± 0.1	7.05 ± 0.07	7.0 ± 0.1
9.30 ± 0.05	9.8 ± 0.1	0.6 ± 0.1	8.55 ± 0.07	8.6 ± 0.1

[a]In all cases the scattering contribution is neglected, $p = 0$; the size of the rod $\varnothing = 350$ μm, and the diffusion constant inside the rod $D_2 \ll D_1$. The absorption parameter α was used as a free-fitting parameter.

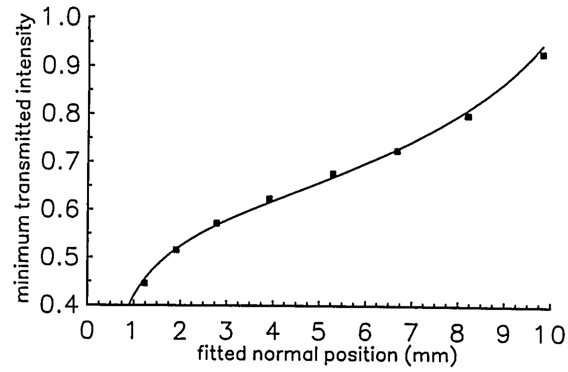

Fig. 6. Minima of the intensity profiles for different positions of the absorbing wire. The experimental points of Table 1 are plotted. The solid curve is obtained from Eq. (25) with $L = 10.0$ mm, $a = 0.175$ mm, $D_1/\alpha a = 1.00$, $p = 0$, and $D_2 = 0$.

Table 2. Fits of the Calculated Line Shape to Transmission Experiment Data[a]

Experimental Transversal Displacement (mm)	Fitted Transversal Displacement (mm)
2.00 ± 0.02	2.05 ± 0.03
4.00 ± 0.02	4.04 ± 0.06
5.00 ± 0.02	5.02 ± 0.07
7.00 ± 0.02	7.03 ± 0.09
9.00 ± 0.02	9.1 ± 0.1
11.00 ± 0.02	11.1 ± 0.2

[a]Experimental displacements of an absorbing rod parallel to the slab are compared with those obtained from the corresponding fits. The distance between the rod and the boundary (x position) is 4.30 ± 0.02 mm, and the thickness of the cell is 10.0 mm. The scattering contribution is neglected ($p = 0$), and the diffusion constant inside the rod is small ($D_2 \ll D_1$). In all cases the relative absorption strength $D_1/\alpha a = 1.4 \pm 0.1$.

strength are adjustable fit parameters. The size of the rod was fixed at the physical diameter in the expression for q (Eq. 24), the diffusion constant inside the object can be neglected with respect to the surrounding medium, $D_2 \ll D_1$, and the dipole contribution, which is a^2/L^2 times smaller than the charge term, is also neglected. All theoretical curves are convoluted with the experimental spatial resolution. The agreement between measured and calculated profiles is excellent. We derive from the fits the positions of the objects; the minimum (or maximum) gives us the y position, and the width of the profile reflects the depth (x position) of the object.

In Table 1 we compare the experimental distances between the boundary and the absorbing rod with the distances obtained from the numerical fits of Eq. (25) to the measured line shapes. There is a systematic error in the normal position determination. An explanation can be found in experimental errors that are still present even after careful alignment of the optical components. Image faults of the intensity profile on the diode array are caused by the lens but are also caused by a small misalignment of the rod with respect to the diode array. Reflection inside the 20-mm-thick windows will still give a slight deformation of the intensity profile. All these effects smear the intensity profile, and therefore the apparent position of the object will correspond to a position deeper inside the slab than the real position. In the third and fourth columns of Table 1 we have listed the positions of the rod relative to the first position, for the real positions as well as for the obtained position from the corresponding fits. When we compare these columns, we conclude that the disagreement is less than 100 μm and is comparable with the experimental uncertainty.

From the strength of the intensity profile (the peak height relative to the background) one can derive the charge of the rod, and from the charge one should be able to recover the size of the rod. The charge also depends on the unknown absorbing parameter α. Only for black materials, which are hard to find in a tractable shape, does this minimum value become independent of α. But still an experimental investigation on the size dependence of the charge strength is difficult, because the charge depends logarithmically on the size.

In Fig. 6 we plot the minima of the intensity profiles as a function of the fitted normal position of the absorbing rod. The solid curve is obtained from Eq. (25), with $D_1/\alpha a = 1.00 \pm 0.03$ as the best overall value for the absorbing strength (the last two points, $x_0 = 8.2$ and $x_0 = 9.8$, were not included in the fit). If one also takes the size of the rod as a free-fitting parameter, one obtains $D_1/\alpha a = 2.15 \pm 0.03$ and $a = 0.52 \pm 0.04$. When the experimental instead of the fitted positions are used, one obtains

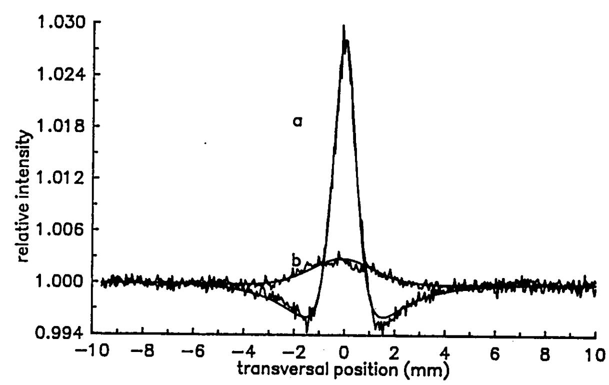

Fig. 7. Transmitted intensity profiles from a cell containing a diffusive scattering suspension for a transparent fiber with $\phi = 350$ μm at different positions inside the cell: a, $x_0 = 0.74 \pm 0.05$; b, $x_0 = 2.5$ mm; $l = 20 \pm 3$ μm, cell thickness $L = 5.0$ mm. Experimental data are shown together with the best numerical fits. The fits are obtained from Eq. (25): a, $x_0 = 0.60 \pm 0.02$ mm, $D_2 = \infty$, $D_1/\alpha a = 1 \times 10^2$; b, $x_0 = 2.4 \pm 0.1$ mm, $D_2 = \infty$, $D_1/\alpha a = 1 \times 10^2$.

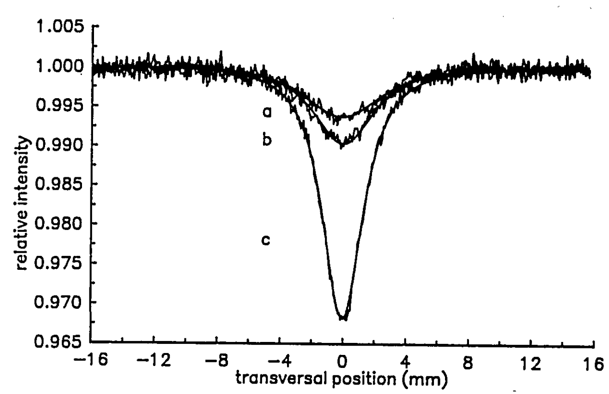

Fig. 8. Backscattered intensity profiles for an absorbing wire $\phi = 350$ μm inside a scattering suspension at different positions: a, $x_0 = 1.68$ mm; b, $x_0 = 1.38$ mm; c, $x_0 = 0.78$ mm. Transport mean-free path $l = 47 \pm 3$ μm, cell thickness $L = 4.0$ mm. Experimental data are shown together with numerical fits for the experimental data from Eq. (26); see also Table 3.

Table 3. Fits of the Calculated Line Shape to Experimental Data Obtained from a Backscatter Experiment with an Absorbing Rod[a]

Experimental Normal Position (mm)	Fitted Normal Position (mm)	Absorption Strength $D_1/\alpha a$
0.28 ± 0.05	0.34 ± 0.02	0.5 ± 0.1
0.78 ± 0.05	0.82 ± 0.02	0.6 ± 0.1
1.38 ± 0.05	1.32 ± 0.02	2.0 ± 0.1
1.68 ± 0.05	1.7 ± 0.1	1.7 ± 0.1
$\Delta x = 50 \pm 5\ \mu m$	$\Delta x = 48 \pm 3\ \mu m$[b]	

[a]The size of the rod $\varnothing = 350\ \mu m$, and the thickness of the cell is 4 mm. The scattering contribution is neglected ($p = 0$). The diffusion constant inside the rod $D_2 \ll D_1$.

[b]The last line in the table illustrates the sensitivity for small displacements of the rod. Two successive scans are taken at 0.650 and 0.655 mm from the boundary. The displacement of only 50 μm is reproduced by the corresponding fits.

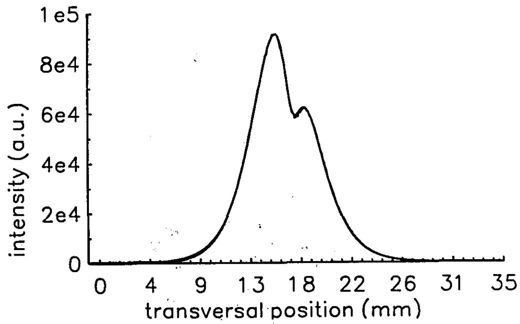

Fig. 9. Measured transmitted intensity from a slablike scattering medium containing an absorbing wire with $\varnothing = 350\ \mu m$. A line source is used instead of a plane wave. Normal position of wire $x_0 = 1.05 \pm 0.05$ mm. Transport mean-free path $l = 20 \pm 3\ \mu m$, cell thickness $L = 5.0$ mm. The smooth curve shows the nunerical fit to the experimental data, $x_0 = 1.03 \pm 0.02$ mm. The fit is derived from Eq. (29).

$D_1/\alpha a = 0.50 \pm 0.03$ and $a = 0.075 \pm 0.04$. In three dimensions the charge depends linearly on the size, so one should be able to obtain more reliable values for the size of the object. Note also that the strength of the charge gives the minimum possible size of the object, because a finite absorption length will always decrease the strength.

In Table 2 displacements parallel to the slab are compared with those obtained from the corresponding fits of Eq. (25) to the measured line shape. The transversal position can be determined with an accuracy of 20 μm, even if the rod is placed far from the boundaries. The slight disagreement between the real position and the position obtained from the fits in Table 2 arises mainly from the curved focal plane of the lens used.

In Fig. 7 we plot the transmitted intensity profiles for a transparent fiber, $\varnothing = 350\ \mu m$, in a cell with thickness 5.0 mm for two different normal positions. Clearly we see the dipole behavior in the disturbance of the transmitted intensity. However, it turned out that no good fits could be made without absorption present. That the fiber can act as a light sink can be understood by considering the finiteness of the sample. Once inside the fiber the light can easily escape the sample by leaking out through the top or the bottom of the cell.

In backscattering we consider only absorbing rods, since the expected intensity profile from the object relative to the total backscattered light from the slab is small. We use a 0.3-mm pencil embedded in a scattering suspension with a transport mean free path of $47 \pm 3\ \mu m$; the cell with the 4-mm windows was used. Results are shown in Fig. 8 together with the best numerical fits. The shapes of the experimentally observed intensity profiles are excellently reproduced by the calculated profiles. The transversal position can be determined with an accuracy of 20 μm. The values for the x positions of the rod, obtained from the fits, are shown in Table 3 and are compared with the experimental positions.

To get an idea about the sensitivity of the profile on the position of the object, we took two successive scans with a displacement of the object of $50 \pm 2\ \mu m$ as the only difference. From the fitted profiles we obtained a displacement of $48 \pm 3\ \mu m$, which is shown in the last line in Table 3.

The last figure, Fig. 9, shows the transmitted intensity profile through a 5-mm-thick sample when a line source is used and an absorbing rod is positioned besides the source. We obtained the fit by taking the derivative of Eq. (29) at the boundary of the slab to determine the transmitted intensity profile. One fits the envelope of the intensity profile by putting the light source one mean-free path inside the slab. Then the strength of the light source is varied to give an optimal fit to the envelope. In addition to the position of the object, the absorption strength must also be fitted to accomplish the final fit.

4. CONCLUSION

We have considered the situation of a single object embedded in a diffusely scattering medium that is confined in a simple geometry, and we have calculated the disturbance on the intensity from this object. We have shown that the object can be located, as long as the object absorbs or if the diffusion constant of the object is different from the embedding medium.

The shape of the intensity profiles is completely determined by the geometry of the surrounding medium and the position of the object. Thus a small object gives a broad profile as a result of diffusional broadening. The calculated profiles are in good agreement with the measured profiles; therefore one can recover small displacements of the object and the transversal position determination in a slab becomes rather simple. The absolute normal position determination is influenced by experimental errors and is of the order of 100 μm. For absorbing objects a minimum possible size can be directly obtained from the strength of the charge term. More information on the size and on the absorption strength can be obtained when the transmitted intensity can be recorded for various normal positions of the object.

The visibility of an object scales with the ratio a/L, a being the object and L the sample size, because diffuse intensity is measured.

ACKNOWLEDGMENTS

The authors thank Shechao Feng for initiating the experiment, Jean-Marc Luck for drawing attention to the application of diffusion theory, and Meint van Albada and Johannes de Boer for helpful discussions. This work is part of the research program of the Stichting voor Fundamenteel Onderzoek der Materie, which is financially supported by Nederlandse Organisatie voor Wetenschappelijk Onderzoek. The work of Nieuwenhuizen has been made possible by a fellowship of the Royal Netherlands Academy of Arts and Sciences.

REFERENCES AND NOTES

1. S. R. Arridge, P. van der Zee, M. Cope, and D. T. Delpy, "Reconstruction methods for infra-red absorption imaging," in *Time-Resolved Spectroscopy and Imaging of Tissues,* B. Chance and A. Katzir, eds., Proc. Soc. Photo-Opt. Instrum. Eng. **1431,** 204–351 (1991).
2. D. T. Delpy, M. Cope, P. van der Zee, S. Wray, and J. Wyatt, "Estimation of optical pathlength through tissue from direct time of flight measurement," Phys. Med. Biol. **33,** 1433–1442 (1988).
3. H. Chen, Y. Chen, D. Dilworth, E. Leith, J. Lopez, and J. Valdmanis, "Two-dimensional imaging through diffusing media using 150-fs gated electronic holography techniques," Opt. Lett. **16,** 487–489 (1991).
4. K. M. Yoo, Q. Xing, and R. R. Alfano, "Imaging objects hidden in highly scattering media using femtosecond second-harmonic-generation cross-correlation time gating," Opt. Lett. **16,** 1019–1021 (1991).
5. R. W. Waynant, presider, session on biomedical imaging, in *Conference on Lasers and Electro-Optics,* Vol. 10 of 1991 OSA Technical Digest Series (Optical Society of America, Washington, D.C., 1991), pp. 101–104.
6. E. N. Leith, C. Chen, H. Chen, Y. Chen, J. Lopez, and P. C. Sun, "Imaging through scattering media using spatial incoherence techniques," Opt. Lett. **16,** 1820–1822 (1991).
7. R. Berkovits and S. Feng, "Theory of speckle-pattern tomography in multiple-scattering media," Phys. Rev. Lett. **65,** 3120–3123 (1990).
8. I. Freund, "Image reconstruction through multiple scattering media," Opt. Commun. **86,** 216–227 (1991).
9. A. Ishimaru, *Wave Propagation and Scattering in Random Media* (Academic, New York, 1978), Vols. I and II.
10. H. C. van de Hulst, *Multiple Light Scattering* (Academic, New York, 1980), Vols. I and II.
11. J. Fishkin, E. Gratton, M. J. van de Ven, and W. W. Mantulin, "Diffusion of intensity modulated near-infrared light in turbid media," in *Time-Resolved Spectroscopy and Imaging of Tissues,* B. Chance and A. Katzir, eds., Proc. Soc. Photo-Opt. Instrum. Eng. **1431,** 122–135 (1991).
12. S. R. Arridge, M. Cope, P. van der Zee, P. J. Hilson, and D. T. Delpy, "Visualization of the oxygenation state of brain and muscle in newborn infants by near infra-red transillumination," in *Information Processing in Medical Imaging,* S. L. Bacharach, ed. (Nijhoff, Dordrecht, 1985), pp. 155–177.
13. E. M. Sevick, B. Chance, J. Leigh, S. Nioka, and M. Maris "Quantitation of time- and frequency-resolved optical spectra for the determination of tissue oxygenation," Ann. Biochem. Exp. Med. **195,** 330–351 (1991).
14. M. B. van der Mark, M. P. van Albada, and A. Lagendijk, "Light scattering in strongly media: multiple scattering and weak localization," Phys. Rev. B **37,** 3575–3592 (1988).
15. See, for instance, J. D. Jackson, *Classical Electrodynamics* (Wiley, New York, 1975).
16. E. Akkermans, P. E. Wolf, and R. Maynard, "Coherent backscattering of light by disordered media: analysis of the peak line shape," Phys. Rev. Lett. **56,** 1471–1474 (1986).
17. See, for instance, J. W. Goodman, *Statistical Optics* (Wiley, New York, 1985).